Progress In Electromagnetics Research, PIER 29, 87–106, 2000

SCATTERING BY AN ARBITRARILY SHAPED ROTATIONALLY UNIAXIAL ANISOTROPIC OBJECT: ELECTROMAGNETIC FIELDS AND DYADIC GREEN'S FUCNTIONS

S. Liu, L. W. Li, M. S. Leong, and T. S. Yeo

Communications and Microwave Division
Department of Electrical Engineering
The National University of Singapore, Singapore 119260

Abstract–The electromagnetic scattering by a three-dimensional arbitrarily shaped rotationally uniaxial anisotropic object is studied. Electromagnetic fields in a uniaxial medium are solved for first using the method of separation of variables, and then expressed in a very compact form by introducing the modified spherical vector wave functions. The equivalence theorem and the T-matrix method are applied in the analysis of the scattering problem. The scattered fields and the dyadic Green's functions both external and internal to the scatterer are derived in terms of spherical vector wave functions and matrix-form coefficients. Through making use of the dyadic Green's functions obtained, numerical results are provided for an incident field excited by an infinitesimal dipole. The scatterers are assumed to be prolate and oblate dielectric spheroids with the rotational z-axis. The angular scattering intensities in far-zone are plotted for all these cases. And some conclusions are also drawn eventually from numerical discussions.

1. INTRODUCTION

The scattering of electromagnetic waves by dielectric objects has for a long time been a hot research topic [1–8]. Knowledge of the scattered fields is required in many areas, such as investigations of the scattering of light by small chemical and biological particles [2] and the scattering of microwaves by raindrops [7]. Quite a few methods have been used in the analysis of different scattering problems (more descriptions can be found in [3]). To study more complex scattering problems, a matrix formulation, which could be classified as an integral equation method, was introduced early by Waterman [1]. This method, using a transition matrix to relate the incident field and the scattered field, is usually called T-matrix (transition matrix) method. A good application of the T-matrix method using the vector wave functions was implemented by Barber and Yeh [3]. The differential scattering characteristics of closed three-dimensional arbitrarily shaped dielectric objects were investigated. Recently, Li et al., [8] extended the method and obtained the dyadic Green's functions for this scattering problem. The T-matrix method is ideally suited for analysing the electromagnetic scattering by nonspherical particles. Although the method is applicable to arbitrarily-shaped particles, it has been applied almost exclusively to axisymmetric particles, i.e., bodies-of-revolution [9–10].

A similar procedure based on the T-matrix method was devised by Lakhtakia et al., to study the electromagnetic response of nonspherical chiral objects exposed to an incident field [4]. But to our knowledge, there's few literature so far on the electromagnetic scattering by arbitrarily shaped anisotropic bodies. The scattering problems involving anisotropic obstacles considered in previous contributions are mostly restricted to planar (or stratified) structures [11], cylinders [5, 12–14], or spheres [6]. This paper concerns with the scattering by a rotationally uniaxial obstacle of arbitrary shape (Fig. 1). In the beginning, the electromagnetic fields in a uniaxial medium are formulated by using the method of the separation of variables and introducing the spherical vector wave functions. In dealing with the scattering problem, the boundary conditions are imposed and the equivalence principle and the T-matrix (transition matrix) method are applied to relate the incident field and the scattered field through the internal field in a matrix form. The electromagnetic fields both internal (denoted by subscript u) and external (denoted by subscript 0) to the scatterer are subsequently obtained and the dyadic Green's functions (DGFs) are derived for the

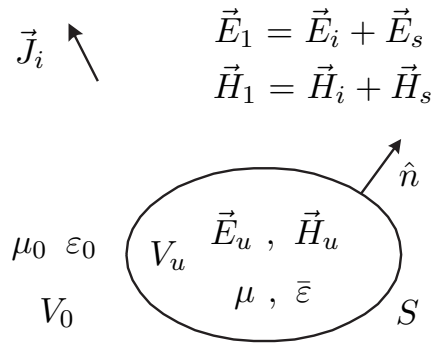

Figure 1. EM radiation due to a source in the presence of an arbitrarily shaped object.

first time. With these obtained dyadic Green's functions, not only the illumination of plane waves, which is usually considered in previous contributions [3, 4], but arbitrary incidences can also be assumed, dependent on where the source point is located and how it is polarized. As applications, numerical examples are given for a dipole radiation in the presence of various uniaxial spheroids.

2. EM FIELDS IN A ROTATIONALLY UNIAXIAL MEDIUM

The characteristic of uniaxial anisotropic media is the existence of a distinguished axis which is usually referred to as optics axis. The element referring to this optics axis is different from the remaining two diagonal ones. The constitutive relations [15] are given by

$$\boldsymbol{D} = \bar{\boldsymbol{\epsilon}} \cdot \boldsymbol{E}, \tag{1a}$$

$$\boldsymbol{B} = \mu \boldsymbol{H}, \tag{1b}$$

where μ is the permeability, and $\bar{\boldsymbol{\epsilon}}$ is a uniaxial tensor given by

$$\bar{\boldsymbol{\epsilon}} = (\epsilon_r - \epsilon_t)\, \hat{\boldsymbol{r}}\hat{\boldsymbol{r}} + \epsilon_t \bar{\boldsymbol{I}}, \tag{2}$$

with the unit dyad $\bar{\boldsymbol{I}} = \hat{\boldsymbol{r}}\hat{\boldsymbol{r}} + \hat{\boldsymbol{\theta}}\hat{\boldsymbol{\theta}} + \hat{\boldsymbol{\phi}}\hat{\boldsymbol{\phi}}$. The permittivity tensor stands for a class of uniaxial anisotropic media which are rotationally symmetric in spherical coordinates system.

Substituting (1) into source-free Maxwell equations, we have for a uniaxial anisotropic medium

$$\boldsymbol{\nabla} \times \boldsymbol{E} = i\omega\mu\boldsymbol{H}, \tag{3a}$$

$$\boldsymbol{\nabla} \times \boldsymbol{H} = -i\omega\bar{\boldsymbol{\epsilon}} \cdot \boldsymbol{E}. \tag{3b}$$

The time harmonic dependence $e^{-i\omega t}$ has been assumed and will be suppressed throughout this paper.

To solve Maxwell's equations, it is more convenient to pose the problem in terms of only the radial functions E_r and H_r [5]. After some lengthy mathematical manipulations, we arrive at a set of second-order differential equations involving only the radial field components:

$$\frac{1}{r^2}\frac{\partial^2}{\partial r^2}\left(r^2 E_r\right) + \frac{\epsilon_t}{\epsilon_r}\frac{1}{r^2\sin\theta}\frac{\partial}{\partial\theta}\left(\sin\theta\frac{\partial}{\partial\theta}E_r\right) + \frac{\epsilon_t}{\epsilon_r}\frac{1}{r^2\sin^2\theta}\frac{\partial^2}{\partial\phi^2}E_r + k_t^2 E_r = 0, \tag{4a}$$

$$\frac{1}{r^2}\frac{\partial^2}{\partial r^2}\left(r^2 H_r\right) + \frac{1}{r^2\sin\theta}\frac{\partial}{\partial\theta}\left(\sin\theta\frac{\partial}{\partial\theta}H_r\right) + \frac{1}{r^2\sin^2\theta}\frac{\partial^2}{\partial\phi^2}H_r + k_t^2 H_r = 0, \tag{4b}$$

where $k_t^2 = \omega^2\mu\epsilon_t$.

From the method of separation of variables, the solutions to (4) can be written in the form [5]

$$\begin{bmatrix} E_r \\ H_r \end{bmatrix} = \sum_{n,m}\begin{bmatrix} B_{\substack{e\\o}nm}\, E_n(r) \\ A_{\substack{e\\o}nm}\, H_n(r) \end{bmatrix} P_n^m(\cos\theta)\begin{matrix}\cos\\ \sin\end{matrix} m\phi, \tag{5}$$

where $A_{\substack{e\\o}nm}$ and $B_{\substack{e\\o}nm}$ are the expansion coefficients that are known for the specified fields. $E_n(r)$ and $H_n(r)$ in (5) are expressed in terms of sperical Bessel functions as follows:

$$E_n(r) = \alpha\frac{1}{r}z_l^{(q)}(k_t r), \tag{6a}$$

$$H_n(r) = -i\eta_r^{-2}\eta_t\alpha\frac{1}{r}z_n^{(q)}(k_t r), \tag{6b}$$

where

$$\alpha = k_r^{-\frac{3}{2}}\sqrt{\frac{2k_t}{\pi}}, \tag{7a}$$

$$k_r = \omega\sqrt{\mu\epsilon_r}, \tag{7b}$$

$$\eta_r = \sqrt{\mu/\epsilon_r}, \tag{7c}$$

$$\eta_t = \sqrt{\mu/\epsilon_t}; \tag{7d}$$

while q stands for the kind of the Bessel functions such that

$$z_n^{(q)}(kr) = \begin{cases} j_n(kr) & q=1 \\ y_n(kr) & q=2 \\ h_n^{(1)}(kr) & q=3 \\ h_n^{(2)}(kr) & q=4 \end{cases}; \tag{8}$$

with l dependent upon the medium parameters in the form

$$l = \left[\frac{\epsilon_t}{\epsilon_r} n(n+1) + \frac{1}{4}\right]^{\frac{1}{2}} - \frac{1}{2}. \tag{9}$$

Substituting (5) back into (3), we have

$$\frac{1}{r\sin\theta}\frac{\partial}{\partial\phi}E_r - \frac{1}{r}\frac{\partial}{\partial r}(rE_\phi) = i\omega\mu H_\theta, \tag{10a}$$

$$\frac{1}{r}\frac{\partial}{\partial r}(rE_\theta) - \frac{1}{r}\frac{\partial}{\partial\theta}E_r = i\omega\mu H_\phi; \tag{10b}$$

and

$$\frac{1}{r\sin\theta}\frac{\partial}{\partial\phi}H_r - \frac{1}{r}\frac{\partial}{\partial r}(rH_\phi) = -i\omega\epsilon_t E_\theta, \tag{11a}$$

$$\frac{1}{r}\frac{\partial}{\partial r}(rH_\theta) - \frac{1}{r}\frac{\partial}{\partial\theta}H_r = -i\omega\epsilon_t E_\phi. \tag{11b}$$

As have been shown in [6], the components of electromagnetic fields can be solved by separating the fields into TE and TM (with respect to $\widehat{\boldsymbol{r}}$) fields. Inserting (5) into (10) and (11), and then solving the equations, we finally end up with

$$E_\theta^{TE} = \mp\,\omega\mu\eta_r^{-2}\eta_t\alpha\sum_{n,m}\frac{A_{e_{o}^{nm}}}{n(n+1)}\frac{m}{\sin\theta}z_n^{(q)}(k_t r)P_n^m(\cos\theta)\begin{matrix}\sin\\\cos\end{matrix}m\phi, \tag{12a}$$

$$E_\phi^{TE} = -\,\omega\mu\eta_r^{-2}\eta_t\alpha\sum_{n,m}\frac{A_{e_{o}^{nm}}}{n(n+1)}z_n^{(q)}(k_t r)\frac{dP_n^m(\cos\theta)}{d\theta}\begin{matrix}\cos\\\sin\end{matrix}m\phi, \tag{12b}$$

$$E_\theta^{TM} = \alpha\sum_{n,m}\frac{B_{e_{o}^{nm}}}{l(l+1)}\frac{\partial[rz_l^{(q)}(k_t r)]}{r\partial r}\frac{dP_n^m(\cos\theta)}{d\theta}\begin{matrix}\cos\\\sin\end{matrix}m\phi, \tag{12c}$$

$$E_\phi^{TM} = \mp\,\alpha\sum_{n,m}\frac{B_{e_{o}^{nm}}}{l(l+1)}\frac{m}{\sin\theta}z_l^{(q)}(k_t r)P_n^m(\cos\theta)\begin{matrix}\sin\\\cos\end{matrix}m\phi; \tag{12d}$$

and

$$H_\theta^{TE}=-i\eta_r^{-2}\eta_t\alpha\sum_{n,m}\frac{A_{\substack{e\\o}nm}}{n(n+1)}\frac{\partial\left[rz_n^{(q)}(k_tr)\right]}{r\partial r}\frac{dP_n^m(\cos\theta)}{d\theta}\begin{matrix}\cos\\\sin\end{matrix}m\phi, \quad (13a)$$

$$H_\phi^{TE}=\pm i\eta_r^{-2}\eta_t\alpha\sum_{n,m}\frac{A_{\substack{e\\o}nm}}{n(n+1)}\frac{\partial\left[rz_n^{(q)}(k_tr)\right]}{r\partial r}\frac{dP_n^m(\cos\theta)}{d\theta}\begin{matrix}\cos\\\sin\end{matrix}m\phi, \quad (13b)$$

$$H_\theta^{TM}=\pm i\omega\epsilon_t\alpha\sum_{n,m}\frac{B_{\substack{e\\o}nm}}{l(l+1)}\frac{m}{\sin\theta}z_l^{(q)}(k_tr)P_n^m(\cos\theta)\begin{matrix}\sin\\\cos\end{matrix}m\phi, \quad (13c)$$

$$H_\phi^{TM}=i\omega\epsilon_t\alpha\sum_{n,m}\frac{B_{\substack{e\\o}nm}}{l(l+1)}\frac{m}{\sin\theta}z_l^{(q)}(k_tr)P_n^m(\cos\theta)\begin{matrix}\sin\\\cos\end{matrix}m\phi. \quad (13d)$$

Purposely grouping TE field and TM field for electric and magnetic fields, respectively, and introducing the spherical vector wave functions, we have from (5), (12) and (13)

$$\begin{aligned}\boldsymbol{E}&=\boldsymbol{E}^{TE}+\boldsymbol{E}^{TM}\\&=\omega\epsilon_r\eta_t\alpha\sum_{n,m}\frac{1}{n(n+1)}\left[A_{\substack{e\\o}nm}\boldsymbol{M}_{\substack{e\\o}nm}^{(q)}(k_tr)+B_{\substack{e\\o}nm}\boldsymbol{N}_{\substack{e\\o}ml}^{(q)}(k_tr)\right], \quad (14a)\\\boldsymbol{H}&=\boldsymbol{H}^{TE}+\boldsymbol{H}^{TM}\\&=-i\omega\epsilon_r\alpha\sum_{n,m}\frac{1}{n(n+1)}\left[B_{\substack{e\\o}nm}\boldsymbol{M}_{\substack{e\\o}ml}^{(q)}(k_tr)+A_{\substack{e\\o}nm}\boldsymbol{N}_{\substack{e\\o}nm}^{(q)}(k_tr)\right]. \quad (14b)\end{aligned}$$

The spherical vector wave functions used above are given by [16]

$$\begin{aligned}\boldsymbol{M}_{\substack{e\\o}m\gamma}^{(q)}(k)=&\mp\frac{mz_\gamma^{(q)}(kr)}{\sin\theta}P_n^m(\cos\theta)\begin{matrix}\sin\\\cos\end{matrix}m\phi\,\widehat{\boldsymbol{\theta}}\\&-z_\gamma^{(q)}(kr)\frac{dP_n^m(\cos\theta)}{d\theta}\begin{matrix}\cos\\\sin\end{matrix}m\phi\,\widehat{\boldsymbol{\phi}}, \quad (15a)\\\boldsymbol{N}_{\substack{e\\o}m\gamma}^{(q)}(k)=&\frac{\gamma(\gamma+1)z_\gamma^{(q)}(kr)}{kr}P_n^m(\cos\theta)\begin{matrix}\cos\\\sin\end{matrix}m\phi\,\widehat{\boldsymbol{r}}\\&+\frac{\partial\left[rz_\gamma^{(q)}(kr)\right]}{kr\partial r}\frac{dP_n^m(\cos\theta)}{d\theta}\begin{matrix}\cos\\\sin\end{matrix}m\phi\,\widehat{\boldsymbol{\theta}}\\&\mp\frac{m}{\sin\theta}\frac{\partial\left[rz_\gamma^{(q)}(kr)\right]}{kr\partial r}P_n^m(\cos\theta)\begin{matrix}\sin\\\cos\end{matrix}m\phi\,\widehat{\boldsymbol{\phi}}, \quad (15b)\end{aligned}$$

where γ should be replaced by n or l accordingly when the functions are actually employed in (14). In derivation of (14), the following identity is used:

$$l(l+1) = \frac{\epsilon_t}{\epsilon_r} n(n+1). \tag{16}$$

To further simplify the expressions of electromagnetic fields, it is reasonable to incorporate all the coefficients into $A_{\substack{e\\o}nm}$ and $B_{\substack{e\\o}nm}$ except that the normalized spherical constant is extracted. The final expressions are

$$\boldsymbol{E} = \sum_{n,m} \mathcal{D}_{nm} \left[A_{\substack{e\\o}nm} \boldsymbol{M}^{(q)}_{\substack{e\\o}nm}(k_t r) + B_{\substack{e\\o}nm} \boldsymbol{N}^{(q)}_{\substack{e\\o}ml}(k_t r) \right], \tag{17a}$$

$$\boldsymbol{H} = -\frac{i}{\eta_t} \sum_{n,m} \mathcal{D}_{nm} \left[B_{\substack{e\\o}nm} \boldsymbol{M}^{(q)}_{\substack{e\\o}ml}(k_t r) + A_{\substack{e\\o}nm} \boldsymbol{N}^{(q)}_{\substack{e\\o}nm}(k_t r) \right], \tag{17b}$$

where the spherical normalized constant is defined as

$$\mathcal{D}_{nm} = \frac{\epsilon_m (2n+1)(n-m)!}{4n(n+1)(n+m)!}, \quad \epsilon_m = \begin{cases} 1, & m = 0; \\ 2, & m > 0. \end{cases} \tag{18}$$

Once the field is specified, $A_{\substack{e\\o}nm}$ and $B_{\substack{e\\o}nm}$ become known.

In our study, the origin of the coordinates is located inside the scatterer, so the spherical Bessel function of the first kind should be chosen in the expression of the spherical vector wave functions. And for convenience, we adopt from now onwards the subscript ν to stand for $_{\substack{e\\o}nm}$ and λ to stand for $_{\substack{e\\o}lm}$. Thus (17) is rewritten as follow:

$$\boldsymbol{E} = \sum_{n,m} \mathcal{D}_{nm} \left[a_\nu \boldsymbol{M}^{(1)}_\nu(k_t r) + b_\nu \boldsymbol{N}^{(1)}_\lambda(k_t r) \right], \tag{19a}$$

$$\boldsymbol{H} = -\frac{i}{\eta_t} \sum_{n,m} \mathcal{D}_{nm} \left[b_\nu \boldsymbol{M}^{(1)}_\lambda(k_t r) + a_\nu \boldsymbol{N}^{(1)}_\nu(k_t r) \right]. \tag{19b}$$

3. EQUIVALENCE PRINCIPLE

Making use of Schelkunoff's equivalence principle [3, 4] we can separate the total problem into two parts, external problem and internal problem with respect to the boundary surface of the scatterer. The

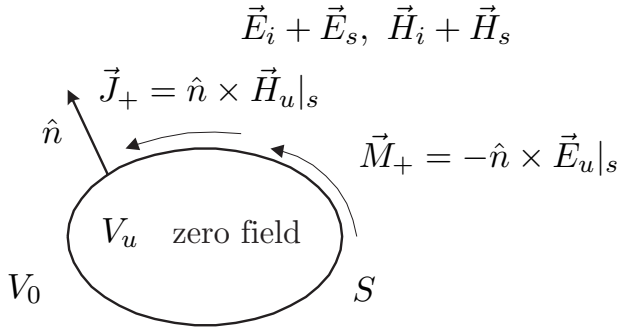

Figure 2. The equivalent external problem.

equivalent surface currents $\boldsymbol{J}_+$ and $\boldsymbol{M}_+$ on the surface of the scatterer produce the total field external to the scatterer and zero field inside the scatterer (Fig. 2). The equivalent surface currents $\boldsymbol{J}_-$ and $\boldsymbol{M}_-$ produce the same field internal to the scatterer as that of the original problem and zero field outside the scatterer (Fig. 3).

In this way, a set of equivalent current sources on the surface of the scatterer replace the actual sources of the field, and the original problem is replaced by two simpler problems.

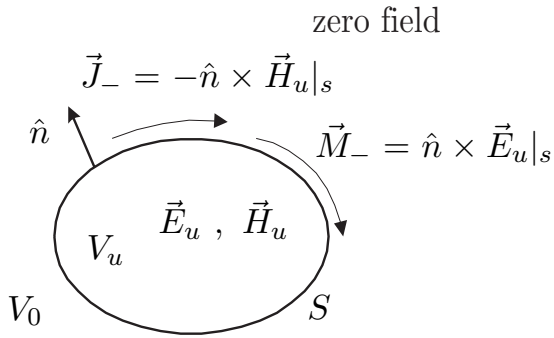

Figure 3. The equivalent internal problem.

4. T-MATRIX METHOD AND DGFs

In this section, the T-matrix method is applied to relate the incident field and the scattered field through the internal transmitted field.

In the region outside the scatterer, the total field is the sum of the incident and the scattered fields, i.e.,

$$\boldsymbol{E}(\boldsymbol{r}) = \boldsymbol{E}_i(\boldsymbol{r}) + \boldsymbol{E}_s(\boldsymbol{r}), \quad \boldsymbol{r} \in V_0 \tag{20}$$

where the incident field $\boldsymbol{E}_i$ and the scattered field $\boldsymbol{E}_s$ are expressed respectively by equivalent surface currents as follows [4]

$$\begin{aligned}\boldsymbol{E}_i(\boldsymbol{r}) = &\boldsymbol{\nabla} \times \int_S \boldsymbol{M}_+(\boldsymbol{r}_s) \cdot \overline{\boldsymbol{G}}(k_0\boldsymbol{R})dS \\ &+ \boldsymbol{\nabla} \times \boldsymbol{\nabla} \times \int_S \frac{1}{i\omega\epsilon_0}\boldsymbol{J}_+(\boldsymbol{r}_s) \cdot \overline{\boldsymbol{G}}(k_0\boldsymbol{R})dS, \quad \boldsymbol{r} \in V_u\end{aligned} \tag{21}$$

and

$$\begin{aligned}\boldsymbol{E}_s(\boldsymbol{r}) = &-\boldsymbol{\nabla} \times \int_S \boldsymbol{M}_+(\boldsymbol{r}_s) \cdot \overline{\boldsymbol{G}}(k_0\boldsymbol{R})dS \\ &- \boldsymbol{\nabla} \times \boldsymbol{\nabla} \times \int_S \frac{1}{i\omega\epsilon_0}\boldsymbol{J}_+(\boldsymbol{r}_s) \cdot \overline{\boldsymbol{G}}(k_0\boldsymbol{R})dS, \quad \boldsymbol{r} \in V_0\end{aligned} \tag{22}$$

where subscript s denotes the surface S of the scatterer, $\boldsymbol{R} = \boldsymbol{r} - \boldsymbol{r}_s$, $k_0 = \omega\sqrt{\mu_0\epsilon_0}$, and $\overline{\boldsymbol{G}}(k_0\boldsymbol{R})$ is the dyadic Green's function in isotropic media, i.e.,

$$\begin{aligned}\overline{\boldsymbol{G}}(k_0\boldsymbol{R}) = \frac{ik_0}{\pi}\sum_{n,m} D_{nm} \Big[&\boldsymbol{M}_\nu^{(3)}(k_0\boldsymbol{r}_>)\boldsymbol{M}_\nu^{(1)}(k_0\boldsymbol{r}_<) \\ &+\boldsymbol{N}_\nu^{(3)}(k_0\boldsymbol{r}_>)\boldsymbol{N}_\nu^{(1)}(k_0\boldsymbol{r}_<)\Big],\end{aligned} \tag{23}$$

where $\boldsymbol{r}_>$ (or $\boldsymbol{r}_<$) is the larger (or smaller) of $\boldsymbol{r}$ and $\boldsymbol{r}_s$.

According to the boundary conditions, the equivalent surface currents in (21) and (22) are given by

$$\boldsymbol{J}_+ = \widehat{\boldsymbol{n}} \times \boldsymbol{H}_+ = \widehat{\boldsymbol{n}} \times \boldsymbol{H}_-, \tag{24a}$$

$$\boldsymbol{M}_+ = -\widehat{\boldsymbol{n}} \times \boldsymbol{E}_+ = -\widehat{\boldsymbol{n}} \times \boldsymbol{E}_-, \tag{24b}$$

where $\widehat{\boldsymbol{n}}$ is the unit outward normal on S, and $\boldsymbol{E}_+$ ($\boldsymbol{E}_-$) and $\boldsymbol{H}_+$ ($\boldsymbol{H}_-$) are the values of the external (internal) $\boldsymbol{E}$ and $\boldsymbol{H}$ fields on the surface, respectively [3].

The incident field in (21) and the scattered field in (22) can be related directly to the source through

$$\boldsymbol{E}_i(\boldsymbol{r}) = i\omega\mu_0 \int_V \overline{\boldsymbol{G}}_0^E(\boldsymbol{r},\boldsymbol{r}') \cdot \boldsymbol{J}(\boldsymbol{r}')dV', \tag{25}$$

and

$$\boldsymbol{E}_s(\boldsymbol{r}) = i\omega\mu_0 \int_V \overline{\boldsymbol{G}}_s^E(\boldsymbol{r},\boldsymbol{r}') \cdot \boldsymbol{J}(\boldsymbol{r}')dV', \tag{26}$$

where the well-known $\overline{\boldsymbol{G}}_0^E$ is given by

$$\begin{aligned}\overline{\boldsymbol{G}}_0^E(\boldsymbol{r},\boldsymbol{r}') = & -\frac{1}{k_0^2}\widehat{\boldsymbol{r}}\widehat{\boldsymbol{r}}\delta(\boldsymbol{r}-\boldsymbol{r}') \\ & + \frac{ik_0}{\pi}\sum_{n,m}\mathcal{D}_{nm}\Big[\boldsymbol{M}_\nu^{(1)}(k_0\boldsymbol{r})\boldsymbol{M}_\nu^{(3)}(k_0\boldsymbol{r}') \\ & + \boldsymbol{N}_\nu^{(1)}(k_0\boldsymbol{r})\boldsymbol{N}_\nu^{(3)}(k_0\boldsymbol{r}')\Big], \quad \boldsymbol{r}\in V_0\end{aligned} \tag{27}$$

and $\overline{\boldsymbol{G}}_s^E$ can be expanded as

$$\begin{aligned}\overline{\boldsymbol{G}}_s^E(\boldsymbol{r},\boldsymbol{r}') = & \frac{ik_0}{\pi}\sum_{n,m}\mathcal{D}_{nm}\Big[\boldsymbol{M}_\nu^{(3)}(k_0\boldsymbol{r})\boldsymbol{a}_\nu(k_0\boldsymbol{r}') \\ & + \boldsymbol{N}_\nu^{(3)}(k_0\boldsymbol{r})\boldsymbol{b}_\nu(k_0\boldsymbol{r}')\Big],\end{aligned} \tag{28}$$

with unknown vectors $\boldsymbol{a}_\nu$ and $\boldsymbol{b}_\nu$ to be determined from boundary conditions, valid for the region where the observation point $\boldsymbol{r}$ is greater than the maximum source distance $\boldsymbol{r}_{s,\max}$ on the object surface.

Substituting (25), (26) and (24) into (21) and (22), taking note that $\boldsymbol{E}_-$ ($\boldsymbol{H}_-$) is just the value of $\boldsymbol{E}$ ($\boldsymbol{H}$) in (19) on the surface of the scatterer regarding which the analytic continuity has been well-documented in [1, 3], hence will not be discussed here but will be considered in numerical computations where $\boldsymbol{r} > \boldsymbol{r}_{s,\max}$, we have after some mathematical manipulations,

$$\begin{bmatrix}\boldsymbol{a}_\nu(k_0\boldsymbol{r}') \\ \boldsymbol{b}_\nu(k_0\boldsymbol{r}')\end{bmatrix} = [T]\begin{bmatrix}\boldsymbol{M}_\nu^{(3)}(k_0\boldsymbol{r}') \\ \boldsymbol{N}_\nu^{(3)}(k_0\boldsymbol{r}')\end{bmatrix}. \tag{29}$$

The transition matrix (T-matrix) $[T]$ is given by

$$[T] = -\begin{bmatrix}I_{1\nu\nu'} & J_{1\nu\lambda'} \\ K_{1\nu\nu'} & L_{1\nu\lambda'}\end{bmatrix}\begin{bmatrix}I_{3\nu\nu'} & J_{3\nu\lambda'} \\ K_{3\nu\nu'} & L_{3\nu\lambda'}\end{bmatrix}^{-1}, \tag{30}$$

where

$$I_{3\nu\nu'} = \int_S dS \left[-\frac{i}{\eta_0} \widehat{\boldsymbol{n}} \times \boldsymbol{M}^{(1)}_{\nu'}(k_t \boldsymbol{r}_s) \cdot \boldsymbol{N}^{(3)}_{\nu}(k_0 \boldsymbol{r}_s) + \frac{i}{\eta_t} \widehat{\boldsymbol{n}} \times \boldsymbol{N}^{(1)}_{\nu'}(k_t \boldsymbol{r}_s) \cdot \boldsymbol{M}^{(3)}_{\nu}(k_0 \boldsymbol{r}_s) \right], \tag{31a}$$

$$J_{3\nu\lambda'} = \int_S dS \left[-\frac{i}{\eta_0} \widehat{\boldsymbol{n}} \times \boldsymbol{N}^{(1)}_{\lambda'}(k_t \boldsymbol{r}_s) \cdot \boldsymbol{N}^{(3)}_{\nu}(k_0 \boldsymbol{r}_s) + \frac{i}{\eta_t} \widehat{\boldsymbol{n}} \times \boldsymbol{M}^{(1)}_{\lambda'}(k_t \boldsymbol{r}_s) \cdot \boldsymbol{M}^{(3)}_{\nu}(k_0 \boldsymbol{r}_s) \right], \tag{31b}$$

$$K_{3\nu\nu'} = \int_S dS \left[-\frac{i}{\eta_0} \widehat{\boldsymbol{n}} \times \boldsymbol{M}^{(1)}_{\nu'}(k_t \boldsymbol{r}_s) \cdot \boldsymbol{M}^{(3)}_{\nu}(k_0 \boldsymbol{r}_s) + \frac{i}{\eta_t} \widehat{\boldsymbol{n}} \times \boldsymbol{N}^{(1)}_{\nu'}(k_t \boldsymbol{r}_s) \cdot \boldsymbol{N}^{(3)}_{\nu}(k_0 \boldsymbol{r}_s) \right], \tag{31c}$$

$$L_{3\nu\lambda'} = \int_S dS \left[-\frac{i}{\eta_0} \widehat{\boldsymbol{n}} \times \boldsymbol{N}^{(1)}_{\lambda'}(k_t \boldsymbol{r}_s) \cdot \boldsymbol{M}^{(3)}_{\nu}(k_0 \boldsymbol{r}_s) + \frac{i}{\eta_t} \widehat{\boldsymbol{n}} \times \boldsymbol{M}^{(1)}_{\lambda'}(k_t \boldsymbol{r}_s) \cdot \boldsymbol{N}^{(3)}_{\nu}(k_0 \boldsymbol{r}_s) \right]; \tag{31d}$$

while $I_{1\nu\nu'}$, $J_{1\nu\lambda'}$, $K_{1\nu\nu'}$ and $L_{1\nu\lambda'}$ take the same form of expressions in (31) except the superscript (3) in (31) should be replaced by (1).

If the fields internal to the scatterer are interested, the dyadic Green's function can also be obtained as follow:

$$\overline{\boldsymbol{G}}^E_u(\boldsymbol{r}, \boldsymbol{r}') = \frac{1}{i\omega\mu} \sum_{n,m} \mathcal{D}_{nm} \left[\boldsymbol{M}^{(1)}_{\nu}(k_t \boldsymbol{r}) \boldsymbol{c}_{\nu}(k_0 \boldsymbol{r}') + \boldsymbol{N}^{(1)}_{\lambda}(k_t \boldsymbol{r}) \boldsymbol{d}_{\nu}(k_0 \boldsymbol{r}') \right], \quad \boldsymbol{r} \in V_u \tag{32}$$

where $\boldsymbol{c}_\nu$ and $\boldsymbol{d}_\nu$ are also given in matrix forms by

$$\begin{bmatrix} \boldsymbol{c}_\nu \\ \boldsymbol{d}_\nu \end{bmatrix} = - \begin{bmatrix} I_{3\nu\nu'} & J_{3\nu\lambda'} \\ K_{3\nu\nu'} & L_{3\nu\lambda'} \end{bmatrix}^{-1} \begin{bmatrix} \boldsymbol{M}^{(3)}_{\nu} \\ \boldsymbol{N}^{(3)}_{\nu} \end{bmatrix} \tag{33}$$

These dyadic Green's functions in (28) and (32) are readily reducible to the case that the scatterer is made of isotropic dielectric material where $\epsilon_r = \epsilon_t$.

5. NUMERICAL RESULTS

As applications of the scattering dyadic Green's function, the scattering by spheroids in free space is considered in this section. Some typical results are presented to show the effects of uniaxial anisotropy on the angular scattering.

For uniaxial media, when $\epsilon_r > \epsilon_t$, we call them positive; otherwise, when $\epsilon_r < \epsilon_t$, we call them negative [6]. In our computation, a positive uniaxial scatter is characterized by $\epsilon_r = 3.0\epsilon_0$ and $\epsilon_t = 2.5\epsilon_0$; while a negative uniaxial scatter is characterized by $\epsilon_r = 3.0\epsilon_0$ and $\epsilon_t = 3.6\epsilon_0$. For convenience in numerical calculation, the permeability of the uniaxial spheroids is set to be μ_0 of free space in all cases.

The surface of a spheroid is described by

$$r(\theta) = \frac{a}{\sqrt{\cos^2\theta + \dfrac{a^2}{b^2}\sin^2\theta}}, \tag{34}$$

where a is its semimajor dimension (along z axis) and b is the radius of its equatorial projection. If $a > b$ the spheroid is prolate, and if $a < b$, it is oblate. In these examples, we choose $a = 0.03\,\mathrm{m}$. For prolate spheroids, $a/b = 3/2$; and for oblate spheroids, $a/b = 2/3$.

Consider an infinitesimal electric dipole in z axis beneath the spheroid shown in Fig. 4. The dipole can be expressed by

$$\boldsymbol{J}(\boldsymbol{r}') = I_p\widehat{\boldsymbol{\theta}}\delta(r' - z_0)\delta(\theta' - \pi)\delta(\phi'), \tag{35}$$

where I_p is the dipole moment, and for ease of computation it is assumed that $\phi' = 0$ due to the symmetry of the problem. The scattered electric field can be calculated using (26).

The solutions to the electric type of dyadic Green's function and electric field are written as infinite sums, but only a finite number of terms can be computed. Enough terms must be included for the fields to converge to an accurate solution with the required accuracy. However, excess terms are to be avoided to save computation time. Due to the assumed source in (35), it is found that all the azimuthal modes m are zero except for $m = 1$. Therefore, m can be set to 1. The value of n depends on the size parameter ka and shape of the particle and is weakly dependent upon the index of refraction [17]. n should be increased both as the shape deviates from that of a sphere and as the size parameter ka increases. In the following calculations,

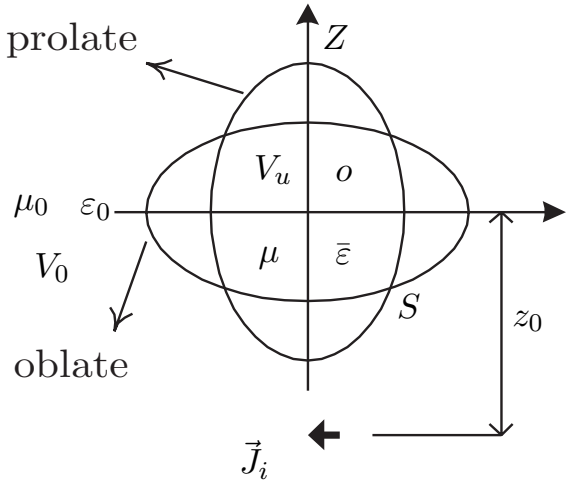

Figure 4. A dipole beneath uniaxial anisotropic spheroids.

n is chosen to be 40 which is large enough for the example cases at $k_0 a = 10$ or less.

The surface integrals $I_{1\nu\nu'}$, $J_{1\nu\lambda'}$, $K_{1\nu\nu'}$, $L_{1\nu\lambda'}$ and $I_{3\nu\nu'}$, $J_{3\nu\lambda'}$, $K_{3\nu\nu'}$, $L_{3\nu\lambda'}$ can be reduced to one-dimensional linear integrals due to the axisymmetry of the scatterer in ϕ dimension. To obtain the far-zone results, we may make use of the following asymptotic expressions [18]:

$$h_n^{(1)}(k_0 r) \approx (-i)^{n+1} \frac{e^{ik_0 r}}{k_0 r}, \tag{36a}$$

$$\frac{1}{k_0 r} \frac{d\left[r h_n^{(1)}(k_0 r)\right]}{dr} \approx (-i)^n \frac{e^{ik_0 r}}{k_0 r}. \tag{36b}$$

Thus asymptotic forms of the vector wave functions in far-zone can be written as

$$\boldsymbol{M}_\nu^{(3)}(k_0) = \frac{(-i)^{n+1}}{k_0} \left[\mp \frac{m}{\sin\theta} P_n^m(\cos\theta) \begin{matrix}\sin \\ \cos\end{matrix} m\phi \, \widehat{\boldsymbol{\theta}} - \frac{dP_n^m(\cos\theta)}{d\theta} \begin{matrix}\cos \\ \sin\end{matrix} m\phi \, \widehat{\boldsymbol{\phi}} \right] \frac{e^{ik_0 r}}{r}, \tag{37a}$$

$$\boldsymbol{N}_{\nu}^{(3)}(k_0) = \frac{(-i)^n}{k_0}\left[\frac{dP_n^m(\cos\theta)}{d\theta}\begin{matrix}\cos\\ \sin\end{matrix} m\phi\,\widehat{\boldsymbol{\theta}}\right.$$
$$\left. \mp\frac{m}{\sin\theta}P_n^m(\cos\theta)\begin{matrix}\sin\\ \cos\end{matrix} m\phi\,\widehat{\boldsymbol{\phi}}\right]\frac{e^{ik_0r}}{r}. \tag{37b}$$

The intensities of the angular scattering in far-zone ($\phi = 0$ plane) are plotted subsequently.

In Fig. 5, the normalized scattered electric field intensities are plotted for positive spheroids with different geometries when $k_0a = 10.0$. It is observed that for the specified point source, when the spheroid is prolate, the field pattern is very smooth. With a/b decreases, which means the spheroid becomes from prolate to oblate, the curve becomes more and more sharply oscillated. The phenomenon can also be observed in Fig. 6, in which negative spheroids are considered. The curve for negative prolate spheroid is much smoother than the other two curves.

Another observation is that at the specified frequency, both positive and negative oblate spheroids generate maximum backward scattering, and the field intensities fall down considerably at the vicinal angular range. This is quite different from the prolate spheroids, by which the angular scattering is very flat that can be seen from the dot curves both in Fig. 5 and Fig. 6.

The difference can also be clearly observed in Fig. 7 and Fig. 8. Although the medium parameters are varied, the shapes of the curves in Fig. 7(or Fig. 8) are quite similar, while the difference between the intensities in Fig. 7 and Fig. 8 is obvious. This is useful for inverse scattering problems when the geometry of the scatterer is concerned. By comparing the three curves in Fig. 7 or Fig. 8, it can be seen that the scattering characteristics of an isotropic spheroid are greatly changed by introducing uniaxial anisotropy although it is only slightly uniaxial ($\epsilon_r/\epsilon_t = 6/5$ or $5/6$).

Form Fig. 9 to Fig. 12, scattered electric field intensities due to some spheroids with different configurations are shown for $k_0a = 2.5,\ 5.0$, and 10.0. Generally, with the frequency increasing, the oscillation of the curve is more and more intensive. But for positive prolate sphroids (Fig. 9), the curves are similar in shape. It means that the frequency responses of this kind of spheroids are smooth over the given frequency range. It can also be seen from these figures that at high frequency, the scattering characteristics are more distinct, which suggests that

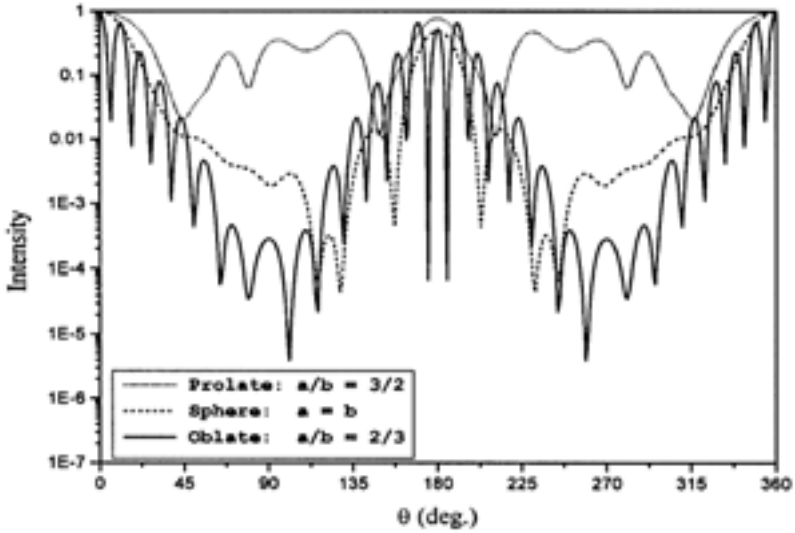

Figure 5. Scattered electric field intensity in $\phi = 0$ plane by positive spheroids: $\epsilon_r = 3.0\epsilon_0$, $\epsilon_t = 2.5\epsilon_0$ and $k_0 a = 10$.

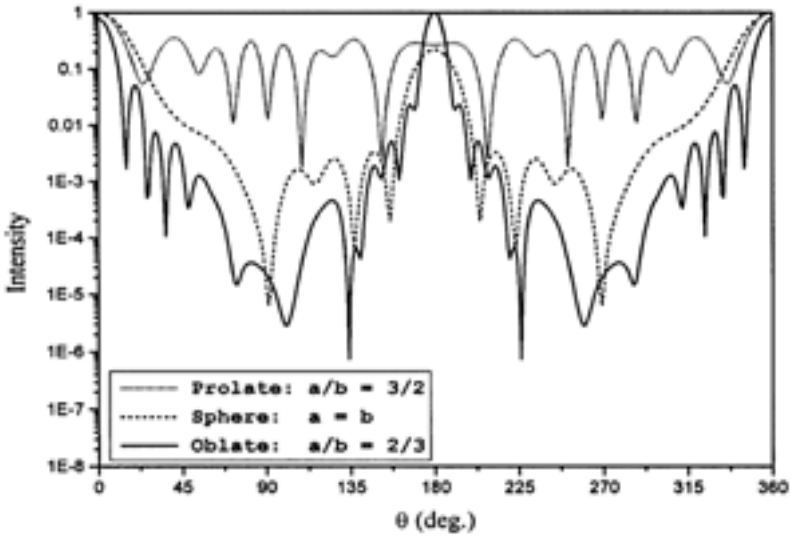

Figure 6. Scattered electric field intensity in $\phi = 0$ plane by negative spheroids: $\epsilon_r = 3.0\epsilon_0$, $\epsilon_t = 3.6\epsilon_0$ and $k_0 a = 10$.

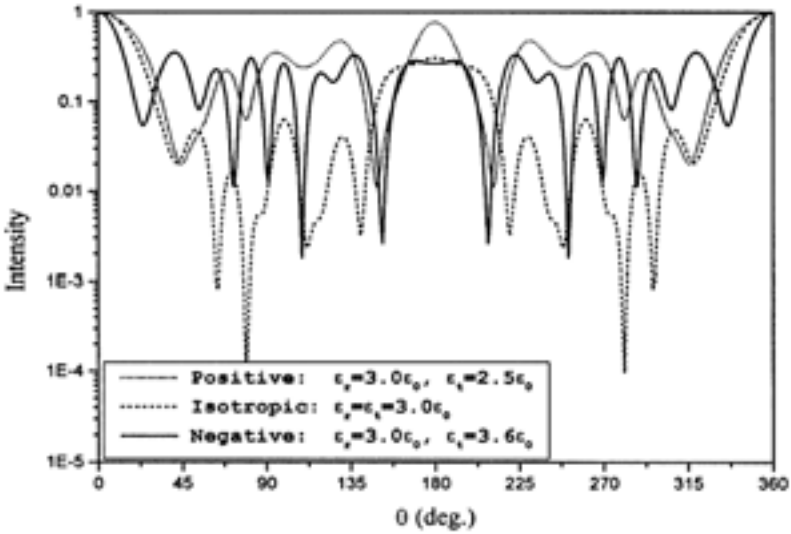

Figure 7. Scattered electric field intensity in $\phi = 0$ plane by prolate spheroids: $a/b = 3/2$ and $k_0 a = 10$.

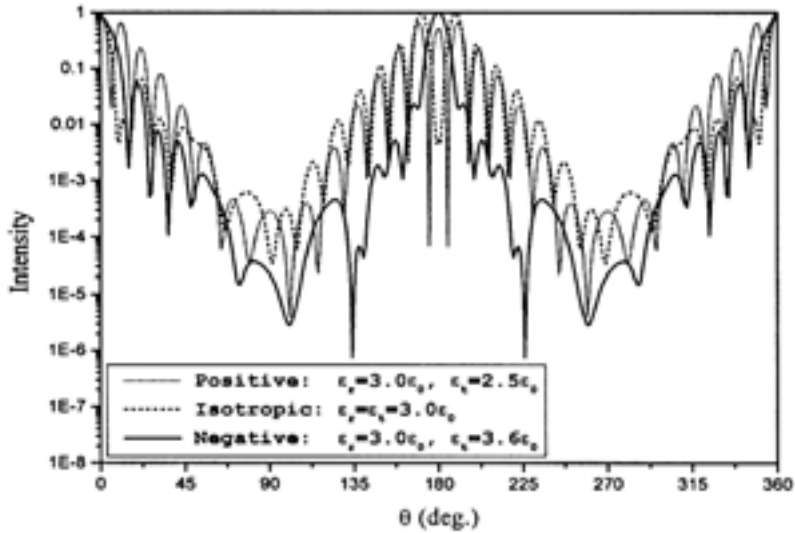

Figure 8. Scattered electric field intensity in $\phi = 0$ plane by oblate spheroids: $a/b = 2/3$ and $k_0 a = 10$.

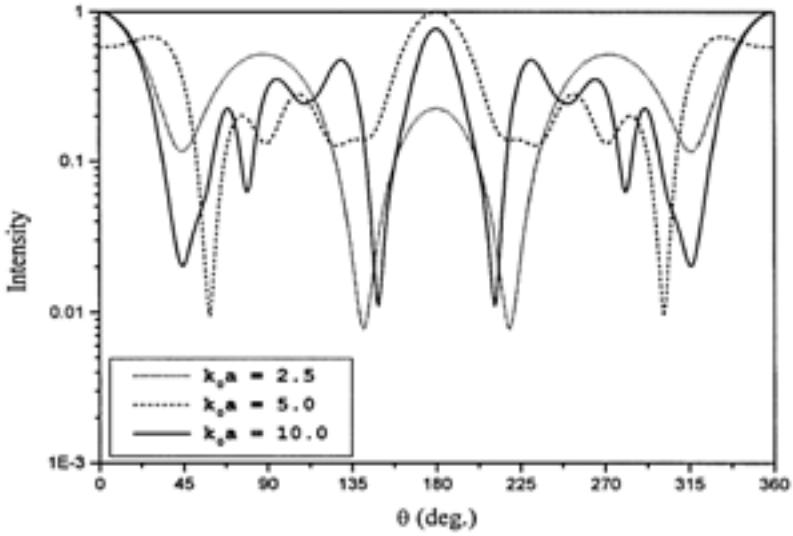

Figure 9. Scattered electric field intensity in $\phi = 0$ plane by positive prolate spheroids at different frequencies: $\epsilon_r = 3.0\epsilon_0$, $\epsilon_t = 2.5\epsilon_0$ and $a/b = 3/2$.

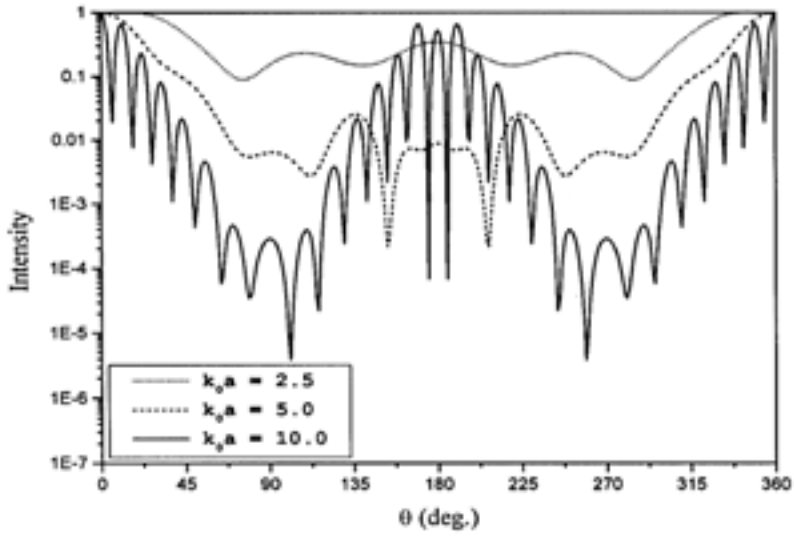

Figure 10. Scattered electric field intensity in $\phi = 0$ plane by positive oblate spheroids at different frequencies: $\epsilon_r = 3.0\epsilon_0$, $\epsilon_t = 2.5\epsilon_0$ and $a/b = 2/3$.

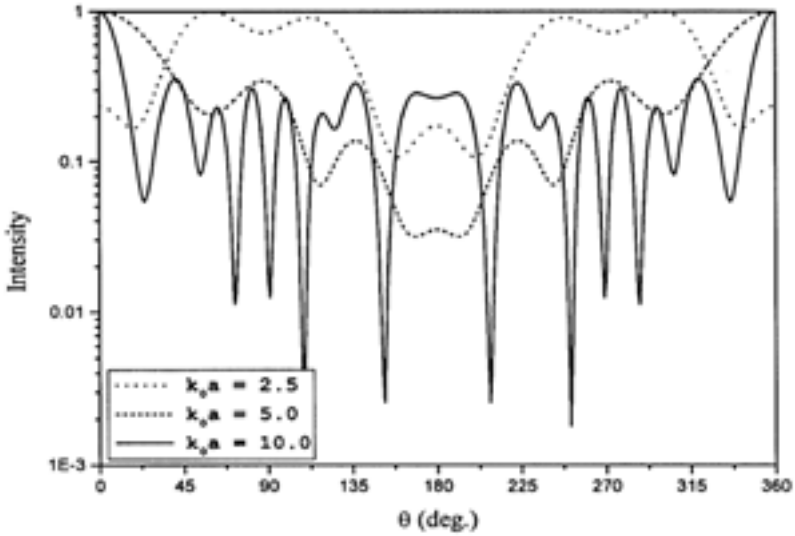

Figure 11. Scattered electric field intensity in $\phi = 0$ plane by positive oblate spheroids at different frequencies: $\epsilon_r = 3.0\epsilon_0$, $\epsilon_t = 3.6\epsilon_0$ and $a/b = 3/2$.

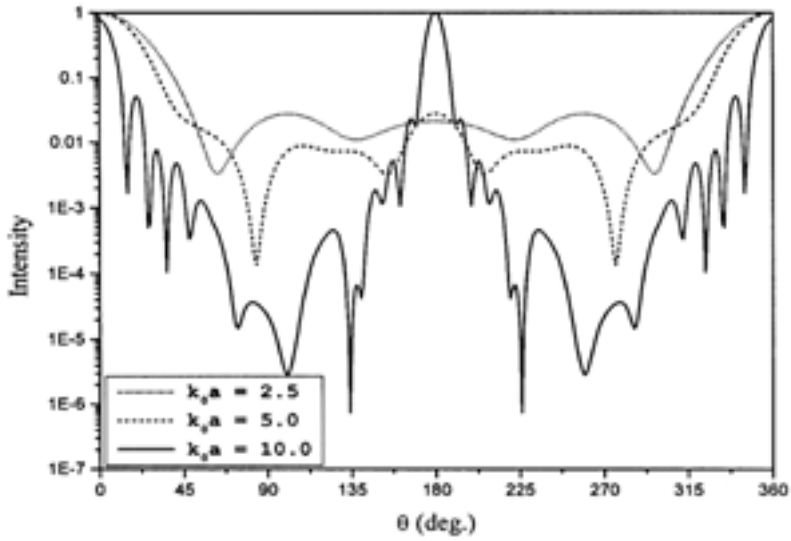

Figure 12. Scattered electric field intensity in $\phi = 0$ plane by positive oblate spheroids at different frequencies: $\epsilon_r = 3.0\epsilon_0$, $\epsilon_t = 3.6\epsilon_0$ and $a/b = 2/3$.

provided the attenuation is in an acceptable extent, the higher the operating frequency, the better the reliability in target recognition.

6. CONCLUSIONS

The electromagnetic scattering by a three-dimensional arbitrarily shaped rotationally uniaxial anisotropic object has been studied. Before dealing with the scattering problem, electromagnetic fields in a uniaxial medium are solved first using the method of separation of variables, and then formulated in terms of the spherical vector wave functions in a very compact form. A procedure based on the T-matrix method is then applied in the analysis of the scattering problem. The scattered field and the incident field are related by imposing the boundary conditions and making use of the equivalence principle. The scattered fields and the dyadic Green's functions both external and internal to the scatterer are derived in terms of spherical vector wave functions and matrix-form coefficients. With the dyadic Green's functions obtained, numerical results are given for an incidence excited by an infinitesimal dipole. The scatterers are assumed to be dielectric spheroids with different configurations: positive uniaxial or negative uniaxial, prolate or oblate, and at different operating frequencies. The angular scattering intensities in far-zone are plotted for all these cases.

REFERENCES

1. Waterman, P. C., "Scattering by dielectric obstacles," *Alta Freq.,* Vol. 38, 348–352, 1969.
2. Bohren, C. F., "Light scattering by an optically active sphere," *Chem. Phys. Lett.,* Vol. 29, 458–462, Dec. 1974.
3. Barber, P. W., and C. Yeh, "Scattering of electromagnetic waves by arbitrarily shaped dielectric bodies," *Appl. Opts.,* Vol. 14(12), 2864–2872, Dec. 1975.
4. Lakhtakia, A., V. V. Varadan, and V. K. Varadan, "Scattering and absorption characteristics of lossy dielectric, chiral, nonspherical objects," *Applied Optics,* Vol. 24, No. 23, 4146–4154, Dec. 1985.
5. Monzon, J. C., "Three-dimensional field expansion in the most general rotationally symmetric anisotropic material: Application to scattering by a sphere," *IEEE Trans. Antennas Propagat.,* Vol. AP-37, No. 6, 728–735, June 1989.

6. Wong, K.-L., and H.-T. Chen, "Electromagnetic scattering by a uniaxially anisotropic sphere," *IEE Proceedings — H,* Vol. 139, No. 4, 314–318, Aug. 1992.
7. Li, L. W., T. S. Yeo, P. S. Kooi, and M. S. Leong, "Microwave specific attenuation by oblate spheroidal raindrops: An exact analysis of tcs's in terms of spheroidal wave functions," in *Progress In Electromagnetics Research, PIER 18,* Jin Au Kong, Ed., Vol. 18, 127–150, 1998.
8. Li, L. W., M. S. Leong, Y. Huang, and T. S. Yeo, "Dyadic Green's functions in the presence of an arbitrarily shaped dielectric object," *9th MINDEF/NUS Joint R & D Seminar,* 37–42, Jan. 1999.
9. Barber, P. W., J. F. Owen, and R. K. Chang, "Resonant scattering for characterization of axisymmetric dielectric objects," *IEEE Trans. Ant. Prop.,* Vol. AP-30, No. 2, 168–172, Feb. 1982.
10. Hill, S. C., A. C. Hill, and P. W. Barber, "Light scattering by size/shape distributions of soil particles and spheroids," *Applied Optics,* Vol. 23, 1025–1031, 1984.
11. Morgan, M. A., D. L. Fisher, and E. A. Milne, "Electromagnetic scattering by stratified inhomogeneous anisotropic media," *IEEE Trans. Ant. Prop.,* Vol. AP-35, No. 2, 191–197, Feb. 1987.
12. Uzunoglu, N. K., P. G. Cottis, and J. G. Fikioris, "Excitation of electromagnetic waves in a pyroelectric cylinder," *IEEE Trans. Ant. Prop.,* Vol. AP-33, No. 1, 90–95, Jan. 1995.
13. Monzon, J. C., and N. J. Damaskos, "Two-dimensional scattering by a homogeneous anisotropic rod," *IEEE Transactions on Antenna and Propagation,* Vol. AP-34, No. 10, 1243–1249, Oct. 1986.
14. Hasan, A. M., and P. L. E. Uslenghi, "Electromagnetic scattering from nonlinear anisotropic cylinders – Part I: fundamental frequency," *IEEE Trans. Ant. Propa.,* Vol. 38, 523–533, 1990.
15. Kong, J. A., *Electromagnetic Wave Theory,* John Wiley & Sons, New York, The 2nd edition, 1986.
16. Tai, C. T., *Dyadic Green's Functions in Electromagnetic Theory,* IEEE Press, Piscataway, New Jersey, The 2nd edition, 1994.
17. Barber, P. W., and S. C. Hill, *Light Scattering by Particles: Computational Methods,* World Scientific, 1990.
18. Stratton, J. A., *Electromagnetic Theory,* McGraw-Will, New York, 1941.